Studies on the Dynamics of Limited Filaments

by

Jeffrey David Bonde

Submitted to the Department of Nuclear Science and Engineering
in partial fulfillment of the requirements for the degree of

Bachelor of Science in Nuclear Science and Engineering

at the

MASSACHUSETTS INSTITUTE OF TECHNOLOGY

September 2010

Author: .....
Jeffrey D. Bonde
Department of Nuclear Science and Engineering
June 3, 2010

Certified and Accepted by: .....
Dennis Whyte
Associate Professor, Nuclear Science and Engineering
Chair, NSE Committee for Undergraduate Studies
Thesis Supervisor

Accepted by: .....
Prof. Jan Egedal
Assisstant Professor, Physics
Thesis Reader

Studies on the Dynamics of Limited Filaments

by

Jeffrey David Bonde

Submitted to the Department of Nuclear Science and Engineering
on June 3, 2010, in partial fulfillment of the
requirements for the degree of
Bachelor of Science in Nuclear Science and Engineering

Abstract

A study on the dynamics of filaments in the presence of a diagnostic, conductive limiter is presented. Plasma filaments are coherent structures present in many fusion devices and transport a significant amount of particles and energy to vacuum chamber walls. The theories of filament propagation are based on a circuit model of current closure loops within the filament and are described herein. Two experimental configurations based on different modes of filament generation are utilized in the Versatile Toroidal Facility (VTF) to test the model. Along with the experimental observations of filament propagation, measurements of limiter sheath resistance are made and shown to depend upon environmental conditions and filament parameters. One experimental configuration creates long filaments ($\sim$6 meters) using electron cyclotron resonance heating (ECRH) and a toroidally symmetric solenoid. The other utilizes a newly constructed Argon plasma gun breaking down injected gas for creating short ($\sim$1 meter) plasma filaments. Arrays of Langmuir probes track the path of the plasma particles while the limiters are constructed to generate a uniform vertical electric field along its conductive side and measure the parallel current collected. Agreement is found with the model in a region of strongly negative vertical electric fields. Current collection data extends agreement to larger regions with eventual breakdown at strongly positive electric fields due to complex current collection and escape paths.

Thesis Supervisor: Prof. Dennis Whyte
Title: Associate Professor, Nuclear Science and Engineering
Chair, NSE committee for Undergraduate Studies

Acknowledgments

There are a few people who have helped me during my undergraduate studies and on this thesis that I would like to acknowledge. I am grateful to Will Fox, Ari Le, and Arturs Vrublesvkis for always being in lab and available for questions and help whenever a bump came in the road. Thanks especially to Noam Katz for his patience and extensive knowledge of systems whenever one of the many questions came up. Thanks to Anthony Kesich for introducing me to these wonderful people. I would like to thank Professor Dennis Whyte for letting me take a somewhat non-conventional academic path that prepared me for this and future material and for his seemingly unlimited insight and amazing guidance over the years. Finally, I would like to thank Professor Jan Egedal for trusting me with the construction and implementation of the diagnostics and equipment used in these experiments, for the invaluable advice given to me over the years; and for an opportunity of a lifetime that I most certainly will never forget. To all of whom I hope that I can repay in kind for the best part of my years at MIT.

Contents

List of Figures

Chapter 1

Introduction

Plasmas exist ubiquitously in the universe constituting close to 90 percent of the visible matter in the universe. Any system of charged particles that exhibits collective behavior can be treated as a plasma. Examples of terrestrial plasmas include lightning, plasma welding arcs, and fusion devices while the solar wind, the sun and stars, and even galaxies are systems of plasmas on the astrophysical scale. The dynamics of each plasma system are determined by not only external influences but also the complex internal interactions, especially compositional effects, giving rise to collective behaviors. Dynamic processes and system properties are generally described in terms of the three basic plasma parameters: the plasma particle density, n; the temperature, T; and the magnetic field, $\vec{B}$. Strong dependence on the environment and the complexity of interactions causes each system to develop a variety of phenomena.

This thesis will focus on studying the dynamics of a specific phenomenon known as plasma filamentation. The remainder of the first chapter will present the nature of the phenomenon including brief descriptions of its general behavior, its physical characteristics, and the motivations for experimentation. The second chapter will describe the physical apparatuses of the experiment including diagnostics and the experimental method used. Chapter three will present the theory behind plasma filament dynamics and the applied experimental techniques. The remaining chapters will present the culmination of the experimental data and follow up with discussions and conclusions.

1.1 Plasma Filaments

In magnetic fusion machines the region of increased neutral particle density between the core plasma and the vacuum chamber wall is known as the scrape-off-layer (SOL) where turbulent flows are most easily seen. The interface between this boundary layer and the core plasma is very notable for its sheared flow generation and turbulence. The core-SOL interface is one example of where plasma filaments originate. Though the actual mechanism for their generation is still a matter of debate, a piece of the core plasma may bulge out and break off amidst the turbulence. Once these small plasma structures separate from the core plasma, the structure becomes coherent and capable of having its own characteristic dynamics and shape separate from the core plasma.

While under the influence of a guide field, plasma particles will tend to stream along the same magnetic field line. The physics of such is that the newly formed plasma structure with particles flowing along a set of field lines will remain connected to this 'flux tube' as both tube and plasma propagate. The flux tube is how plasma filaments maintain their characteristic profile forming an extended tube of plasma while motion perpendicular to the axis of a flux tube, or cross-field motion, occurs. Such motion could be caused by any number of interactions of the plasma filament with its environment including but not limited to interactions with vacuum chamber walls, the magnetic field, collisions with neutrals, or even gravity [1].

1.2 Motivations

Plasma filaments spontaneously appear near turbulent boundaries especially those seen in tokamak plasma devices [2]. Their radial cross-field motion transports significant amounts of plasma particles, momentum, and energy away from the core plasma decreasing the quality of confinement of the device. Filamentation and its dynamics form conundrums that must be understood to successfully create a controlled nuclear fusion device. Though the theory of their governing dynamics has been extensively

studied, presented in part in the theory section of this thesis, experimental verification of these theories remains limited.

The purpose of this thesis is to present such an experiment on the observations of these plasma filament dynamics in the Versatile Toroidal Facility (VTF) at the Massachusetts Institute of Technology. At VTF, plasma filaments are generated in the toroidal device and allowed to propagate radially. A conductive structure, or limiter, separated into a number of plates is placed in the toroidal path of the plasma imposing various electric fields on the terminal ends of the filaments. The effects of the dynamics are then observed by tracking the plasma particle density and the speed with which the plasma structure propagates through the vacuum chamber. A previous experiment [3] conducted in the same machine and in a similar manner experimentally verified the effect of neutral collisions on propagation. This experiment will expand on observations of dynamics as they pertain to the inclusion of the conductive limiters.

Chapter 2

Experimental Design

2.1 Versatile Toroidal Facility (VTF)

The experiments of this thesis were conducted at the Versatile Toroidal Facility of MIT's Plasma Science and Fusion Center (PSFC) under the supervision of Professor Jan Egedal. VTF was originally built as an experimental tokamak but has since undergone modifications to facilitate studies on the phenomenon known as magnetic reconnection. The changes to the device made by Professor Egedal along with already existing features has also made it a suitable environment for studies on plasma filamentation.

VTF's toroidal main vacuum chamber volume measures about 1 m high with a major radius of .9 meters and a width of 65 cm. The main chamber has 17 radial port extensions spaced 20 degrees apart (with an electrical break in place of the 18th) for diagnostic access to the plasma. For flexibility in construction and positioning of the diagnostic apparatuses, access ports are located on the top and bottom of the machine as well with all ports bolted to the chamber with a rubber vacuum-grade seal. One of the radial port extensions attaches the vacuum pump system capable of maintaining background pressures of argon gas (neutral pressure) as low as 10^{-6} Torr (1 Pa $\approx 7.5 \times 10^{-3}$ Torr) referred to as a vacuum.

For the purpose of this thesis, the magnetic field produced is purely toroidal. The toroidal field is generated in VTF by 18 large external coils azimuthally spaced as

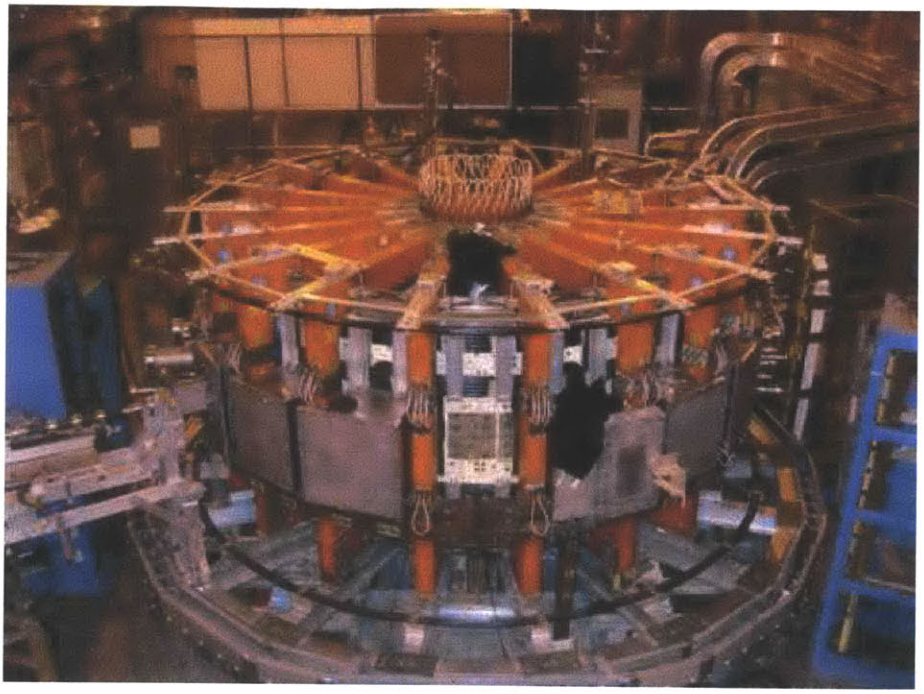

Figure 2-1: Exterior photograph of VTF with orange toroidal magnetic coils and showing a few of the rectangular radial port extensions. This particular photograph also has the view of the electrical break in the machine front and center. Image taken from Ref. [9]

seen in Fig. 2-1. Power is supplied to the magnets by a 13 kV supply used to generate a field of about 46 mT at the inner wall of the chamber falling off as $\sim 1/R$. The relatively low field is not only necessary for one of the modes of plasma generation presented later in this chapter but ensures consistency due to the reduced power demands.

The parameters listed above give the base dimensions of VTF as originally constructed. Additions since its initial operation are related to the plasma generation schemes including a microwave emitter and interior toroidal solenoid for electron cyclotron resonance heating (ECRH) and an ionized argon gas injector, or argon plasma gun. The implementation of these devices will be the subject of the following two sections.

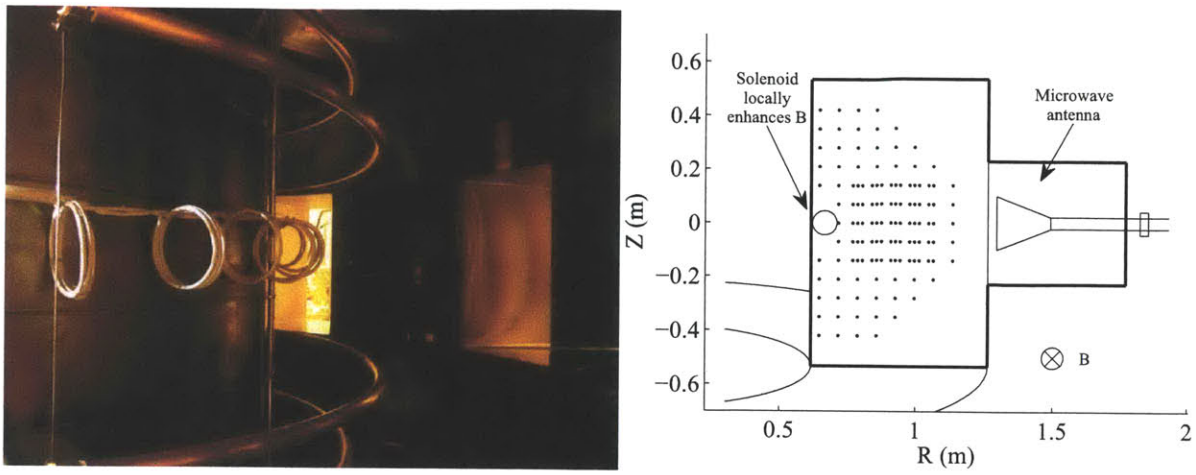

Figure 2-2: Interior photograph, 2-2a, and diagram, 2-2b, of VTF with inner coil used to locally enhance the magnetic field for use in ECRH. Diagram shows gridded langmuir array and microwave horn. Images taken from Ref. [9]

2.2 Plasma Generation by Perturbing Coil (ECRH)

The microwave emitter used on VTF is a klystron amplified source capable of supplying 15 kW of microwave energy at 2.45 GHz. The electron cyclotron frequency linearly depends on the local strength of the magnetic field; $\omega_c = qB/m$, where q is the particle charge and m is the particle mass. Thus, the magnitude of the field must be tuned to facilitate resonant energy transfer between the microwaves and the electrons. Therefore, an internal solenoid wrapped around the inner wall of the vacuum chamber of VTF locally enchances the 46 mT magnetic field to the $\sim$ 87 mT strength required to reach the 2.45 GHz resonance.

The klystron source emits microwaves via a horn at one azimuthal point. The good reflectivity of the interior walls of the vacuum chamber ensures that the power is relatively equally distributed throughout the entire volume. Breakdown occurs inside the interior solenoid where electrons are resonantly stripped from the atoms during the short time the klystron is activated. As the plasma begins to propagate away from the solenoid, the plasma quickly becomes toroidally symmetric as it expands along the field lines at the plasma sound speed, $c_s = \sqrt{T_e/m_i}$. For an argon plasma and typical electron temperatures found in VTF, T_e $\sim$2-15 eV, the sound speed is approximately

2-6 km/s requiring much less than a millisecond to ensure good symmetry in the plasma filament. Figure 2-2 shows the setup of the microwave horn and the inner solenoid.

Because the plasma filament is only partially ionized, the neutral particle population affects the coherence of the plasma filaments generated. If the neutrals are initially at the lower density of $\sim 10^{-6}$ Torr, not enough source neutrals are present to make a resolvable filament by ECRH. At higher neutral pressures, $\sim 10^{-3}$ Torr, the neutrals left over are dense enough to distort the filament shape and dominate over the filament dynamics. Thus, for this plasma generation configuration, the neutral pressure is set in the range of $10^{-5} - 10^{-4}$ Torr ($\sim 10^{17} - 10^{18}$ m^{-3}) to ensure good filament coherence with plasma densities on the order of 10^{16} m^{-3}.

2.3 Plasma Generation by Ion Injection

The other method used in VTF for plasma filament generation is through the newly installed plasma 'gun'. In this setup, a separate source of argon injects gas directly into the vacuum chamber. As the gas enters the chamber, it passes through a region of intense electric field which rips electrons off the atoms. During operation, the gun opens the gas valve for ~50 ms and waiting for steady flow, it arcs during 2 of the last 10 ms releasing a plasma of density on the order of 10^{20} m^{-3} and energies of $\approx$10 eV. The poloidal Toroidal expansion reduces this density closer to that produced by ECRH. Besides the clear benefits of having an initially more dense and hotter plasma, the separate source of neutrals allows for greater flexibility in choosing the neutral pressure in the vacuum chamber. The downside of using this arrangement lies in the time delays of having a point source of plasma in generating a generally toroidal structure.

2.4 Diagnostics

Both methods of filament generation create plasmas of low enough energy density that many of the diagnostics used at VTF are directly inserted into the plasmas. This offers a great advantage over higher energy machines to make very direct measurements with good resolution. More care has to be taken, however, to make sure that the physical scaling of the material placed inside the vacuum chamber does not impede or significantly perturb the plasma structures especially becuase the experiment requires accurate and highly resolved spatial measurements of the plasma particle density. The most basic and effective diagnostic for this purpose at VTF is an electrostatic probe also referred to as a Langmuir probe.

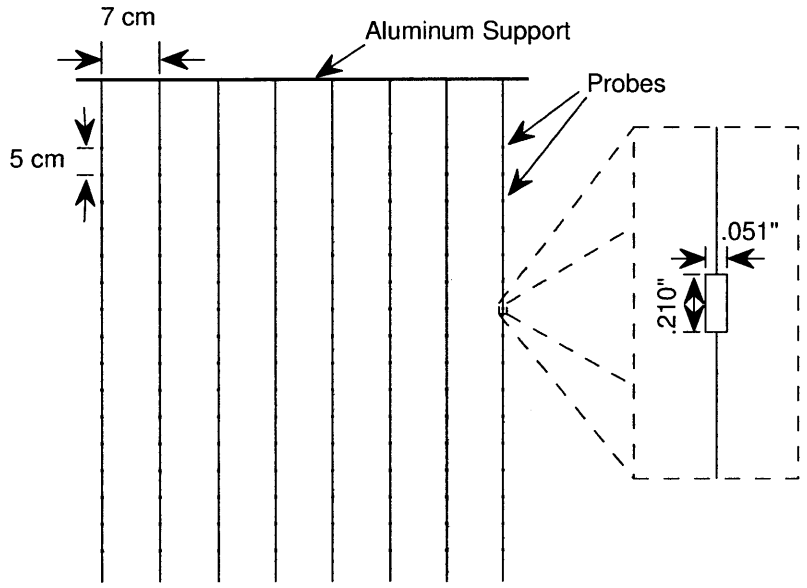

Figure 2-3: Langmuir Array (Hanging): An example of a Langmuir array used in the VTF experiments. This hanging array has 128 stainless steel electrostatic probes arranged in 8 lines of 16 probes spaced at 5 cm vertically and 7 cm horizontally. A single probe is shown in expanded view. The side-loaded array is of similar construction with 12 horizontal rows of 8 probes with 7 cm by 7 cm resolution.

2.4.1 Langmuir Arrays

Arrays of Langmuir probes constitute the major diagnostic on VTF used in filament studies. One array is arranged as a 16×12 grid of probes designed to be mounted radially from a side port spanning the cross section of the vacuum chamber. Three more arrays of 8×16 probes hang from the ports on top of VTF. Though the first array (the "side-loaded" array) has better temporal resolution being digitized at 2 MHz as opposed to 500 kHz, the other three arrays ("hanging arrays") were designed specifically for flexibility in positioning. That is, they may be rearranged relatively quickly while the vacuum seal is broken and moved to different azimuthal angles relative to the side-loaded array and the microwave horn. The side-loaded array was designed with better spatial resolution of 3.5 cm horizontal and 7 cm vertical compared to the hanging arrays' 5 cm by 7 cm resolution.

The construction of all of the Langmuir arrays consist of the individual probes, electrical signal wires, a guide wire, and an aluminum support bar. The signal wiring is a single strand of diameter .003" copper wiring from the California Fine Wire Company connecting each probe to a sealed signal output flange mounted to a port cover. The probes are arranged such that 16 (or 8) probes are mounted onto a single structural line. Due to the small diameter of the copper wiring, an additional wire of diameter .006" supports and anchors the weight of the probes, which are held in place by applying epoxy to the interweaved signal wires. The probes themselves are stainless steel hollowed tubes of outer radius .051" ±.001" hand-cut to a length of .210" ±.005" so that the probes were large enough for reasonably consistent construction but not too big to introduce inhibitive capacitive or perturbative effects on the plasma.

The probes may operate in two modes: biased and floating mode. In *biased* mode, an external potential is applied to probes in the array to collect charged particles and measure local charged particle density whereas in *floating* mode, the probe equilibrates at a potential characteristic of the local plasma potential. The processes involved in making these measurements are described in more detail in the theory section of this thesis. The hanging arrays have been configured such that both float-

ing and biased-moded probes simultaneously operate within each array reducing the overall resolution of a filament but allowing measurement of the electrical characteristics of the filament without additional perturbations. In regular operation, the probes for an entire array may be switched to all biased, all floating, or a number of interleaving floating/biased probe arrangements.

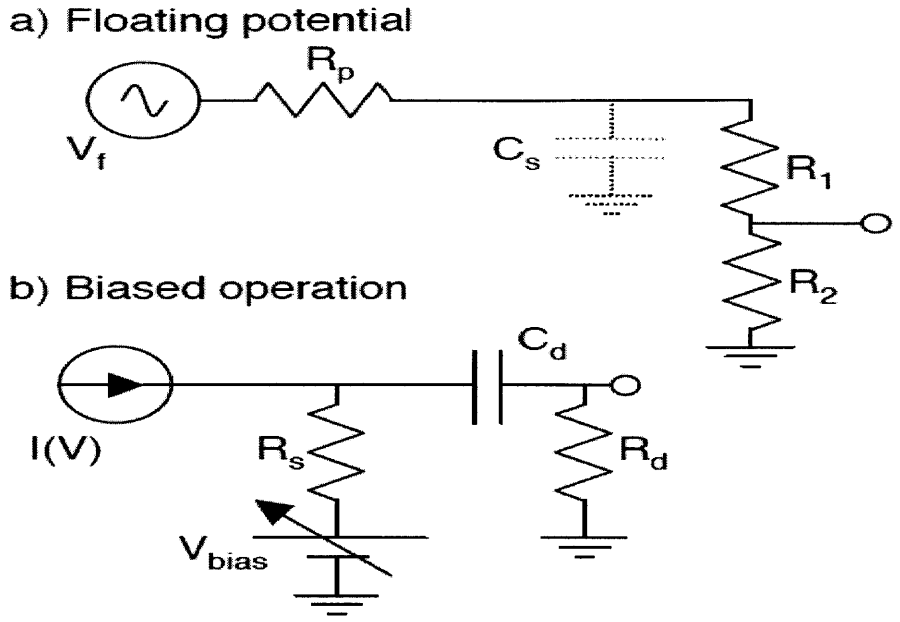

Figure 2-4: Langmuir Operations Circuit: The two separate circuits used to control and digitally read probe operations and data. In (a), R_p and C_s are the resistance and capacitance associated with the probe as it is in contact with the plasma. The resulting voltage is proportioned down by R_1 and R_2 for digitization. In (b), R_s is large so that the ion saturation current is drawn into the digitizer, R_d, and read as a voltage drop. Capacitor C_d acts as voltage protection to the digitizer.

In VTF, the operational modes of the arrays of Langmuir probes are configured via a series of electric circuits and controls as showing in Fig. 2-4. In floating mode, the probes reach the floating potential which is then divided down so that the digitizer safely reads the input signals. For biased mode, the probe's collected current, shielded from the bias source by a large resistor, is read by the subsequent potential drop across the input resistance into the digitizer. First, however, the current is channeled through a capacitor to eliminate the bias voltage from the output to the digitizer. The circuits for each of the floating and biased operation are controlled separately by

a relay circuit. The capacitor in biased operation and the resistor scaling in floating mode are necessary to avoid damaging the digitizers systems which are rated to only handle ± 1 Volt.

Recently at VTF, experiments on plasma filaments with multiple probe arrays set to floating mode have shown an unreliability in the data collected. For a floating probe, the potential it achieves can become limited by the space charge available at 10^{16} m^{-3}. That is, a lack of sufficient local charge to achieve floating potential introduces an increased RC time into the probe circuit (see Fig. 2-4-(a)) and thus a response delay. The experiments also showed a decrease in blob features such as electrical potential and size with the arrays of langmuir probes used for this thesis experiment. Qualitative features of the innermost electrical structure and motion are relatively unaffected but for all intents and purposes, the most interesting quantitative data from floating langmuir probes have been deemed not accurate enough for application to analysis. Provided a good enough power supply is used, the arrays' biased mode of operation is unabated and remains an adequate method to measure the dynamics of filament propagation.

With the combined four langmuir arrays, 704 individual Langmuir probes track the motion of the plasma structures through VTF at a processing rate of either 500 kHz or 2 MHz depending on the digitizers used. Compiling data using Matlab allows easy creation of movie files depicting the time evolution of the isolated plasma filament structures in three dimensions.

2.4.2 Limiters

The base structure of each of the limiters used in the experiment is comprised of 12 printed circuit boards. On almost the entire side of the limiter, the board's surface is exposed copper metal while the other side contains the signal circuitry. The conductive side of a single PCB is split into 8 identical rectangular sections, or plates: 2 independent plates horizontally 7.5 cm in height and 4 electrically independent plates vertically measuring 5.7 cm each. Sets of plastic screws, G10, and aluminum strips on the non-conductive side connect the PCBs into the final limiter structure 3

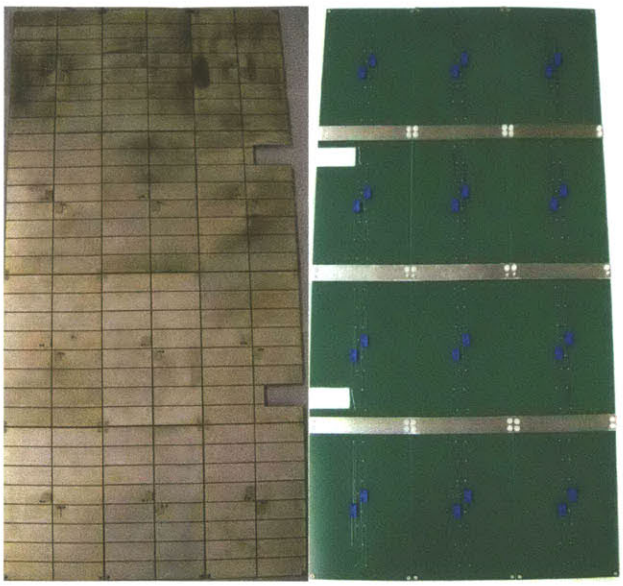

(a) Plasma Facing (b) Electronic Connections

Figure 2-5: Limiter: Photos of limiter construction with 12 individual PCBs connected together. Each PCB has 8 electrically independent exposed copper plates (sectioned into two vertically) with 5.7 cm horizontal and 7.5 cm vertical dimensions. The conductive face (a) and the electronic connections (b).

PCBs wide and 4 PCBs high. The dimensions were chosen to precisely fit into the main vacuum chamber cross-section from just outside the region of filament formation to the outer radial wall. Structural considerations and assembly were such that the limiters could be repositioned azimuthally about the chamber. Two of these wall-like limiters were created to set the plasma filament length and to study the current that such a limiter would draw from the filament.

Sectioning the PCBs of the limiters allows imposing electric fields across the filament ends and drawing current from them. By applying different voltages over an entire limiter, current would be pulled directly out of the filament equivalent to treating it as a voltage supply with a resistor connecting the limiter and plasma. The electrical fields are imposed by creating a potential gradient along the plates with application of 16 roughly evenly spaced potentials. A special power supply had been constructed capable of generating the 16 potentials symmetric about a grounded signal using a large voltage ladder. The potential ladder forms an approximately constant vertical electric field along the height of the limiter and interact with the ends of

the filament. The limiter is connected electronically to digitizers in the same manner as the smaller, more resolving Langmuir probes but used instead to directly measure impinging currents detailing parallel current flow through the filament. Additionally, the currents within the filaments may be measured by a Langmuir probe as well. The construction of the limiters allows such a measurement.

2.5 Experimental Operations Overview

Two slightly different arrangements of the equipment were used to conduct the experiments of this thesis as shown in Fig. 2-6. In the first, the three suspended Langmuir probe arrays and side-loaded array are placed at different toroidal locations. Their separation and simultaneous data acquisition checked the consistency of the filament as the charged particles in the filament not only propagated radially but toroidally as well. The plasma source was the interior solenoid for electron cyclotron heating. The two limiters cut off the formed filament giving it length of ~ 6 m. For each of the experimental discharges performed in this arrangement, a linearly varying potential structure was applied to both of the limiters. During each discharge, the probes would take density measurements which would be used to track the cross-sectional path of the filaments.

For the other arrangement, the main difference is the choice of azimuthal position of the limiters. The choice of a change in limiter position was motivated by the possibility of effects in drift velocity due to the length of the plasma filament between the limiter plates. With the limiters placed about a meter apart, only one of the hanging Langmuir arrays were placed in the path of the filament to limit the perturbative effects. This configuration made use of the plasma gun as a source because the distance between the plates was small enough to allow the filament to become locally symmetric enough for study. This mode of operation not only took data on density but also the resistivity of the sheath layer present where the filament contacts the limiter.

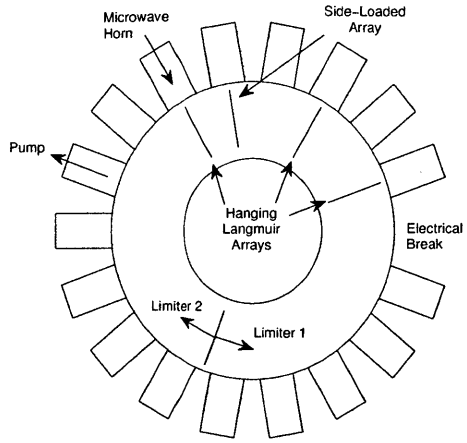

(a) long

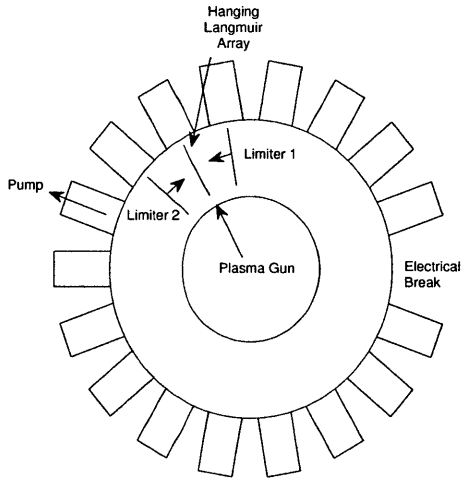

(b) short

Figure 2-6: Configuration: The internal arrangements of the two configurations of diagnostics: (a) is that of the long filaments produced by ECRH and (b) is that of the short filaments produced by argon gun injection.

Chapter 3

Theory

Within the last two decades, fusion scientists have discovered that during standard tokamak operation, a nontrivial amount of particles and their energy are transported radially. Experimental evidence has led researchers to believe that a phenomenon through which this occurs is the formation and propagation of plasma filaments such as those created for this thesis. A new model needed to be developed to explain the anomalous radial transport of these filaments. Professor Sergei Krasheninnikov of the University of California at San Diego, and Doctors Daniel D'Ippolito and James Myra of the Lodestar Research Corporation have led the way in developing the theory behind the dynamics of plasma filaments in tokamak plasma devices. Their theories form the basis of the experiments conducted for this thesis and investigations of filaments in VTF. After a brief theoretical introduction to sheath physics and the physics of Langmuir probes, the basics of their theories on filament propagation, or "blobs" as they call them, are presented.

3.1 Sheath and Langmuir Probe Physics

When a charged particle approaches a conductor, the conducting surface will generate the effect of an image charge by building up a surface charge. The surface charge accelerates the charged particles towards the surface until contact is made neutralizing the particle by recombination resulting in charge removal and increased

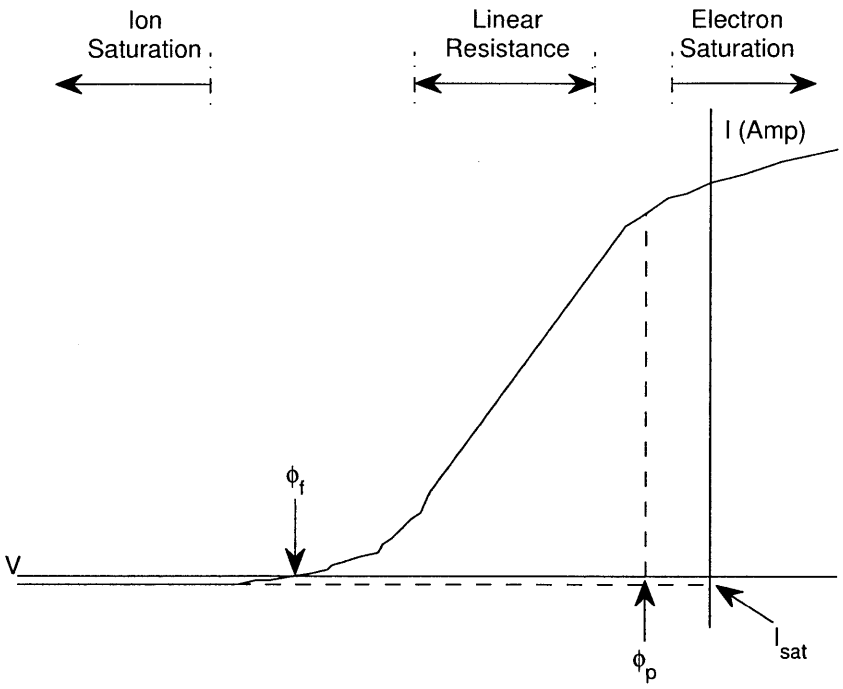

Figure 3-1: Langmuir I-V: The characteristic I-V curve for an electrostatic probe. Just below the region of saturated electron collection is the plasma potential, ϕ_p. On the other end of the region of linear resistance is the floating voltage, ϕ_f, where the current collected is 0; associated with probes in floating mode. In biased mode, V $\ll \phi_f$ to get the ion saturation current, I_{sat}.

potential of the conductor. In systems of many particles and multiple species, the same process occurs except with shielding effects. That is, if one species becomes accelerated towards the conducting surface, the local population decreases and further collection will be reduced by the field of the remaining particles and conductor voltages. In a typical plasma with higher electron temperatures than ion temperatures, $T_e > T_i$, the electrons with higher thermal speeds, $v_T = \sqrt{T/m}$, reach the conductor first establishing an initially negative potential in the material and removing the electrons from the local distribution. An equilbrium is reached when the potential reaches a low enough value such that the electrons are sufficiently reflected and the ions accelerated to have zero net current into the conductor. Local charge distributions and plasma potential place the limits on the potential subsequently induced in the conductor. The steady-state potential acquired when the electron flux equals the

ion flux is known as the floating potential, ϕ_f. Relative to the plasma potential, ϕ_p the floating potential is given by,

$$\phi_f = \phi_p + \frac{T_e}{2e}\left[\ln\left(2\pi\frac{m_e}{m_i}\right) - 1\right] \tag{3.1}$$

which for a singly-charged cold argon plasma with $T_e \approx 2eV$ is approximately -10 Volts. The boundary layer over which the complex charge distribution and electrostatic potential drop form is called the sheath. Sheaths tend to form when the potential of a conductive surface drops $\approx T_e/2e$ below that of the plasma.

The biased mode of the electrostatic probe is used for charged particle density measurement. Since plasmas have such good conductivity, placing a conductive component into a plasma is similar to that of any standard circuit. The associated I-V curve of an electrostatic probe in a plasma is well known and shown in Fig. 3-1. Within a relatively small range of voltages, the probe has a linear response in the plasma, that is, the probe will have a constant resistance. When the voltage applied to the conductor is negative relative to this region, the electrons repel and a sheath dominated by ions forms. If the applied voltage is pushed more and more negative, i.e. $\phi_{probe} - \phi_p \gg T_e/e$, the electrons return to a Maxwellian distribution as approximately no electrons reach the probe surface and all local ions are collected (ion saturation). Thus, as the observation point approaches the probe, the electron density falls by the Boltzmann factor, $e^{(e(\phi-\phi_p)/T_e)}$. Energy conservation assuming cold ions, $T_i \approx 0$, allows the ion flux for a probe of area A_{probe} to be calculated which, by using the quasineutrality condition, $n_i \approx n_e$, just outside the sheath yields the approximate equation for the ion saturation current,

$$I_{sat} = \exp\left(-\frac{1}{2}\right) A_{probe} n_\infty c_s \tag{3.2}$$

Given a measured current into the probe of known dimensions, Eq. (3.2) determines the local plasma density.

3.2 Plasma Filament Dynamics

3.2.1 Dynamics and The Vorticity Equation

The basic foundation of the dynamics of any system is Newton's Laws of Motion. Writing down the 2nd law for particles of a species, α, in an electromagnetic field yields the Lorentz force equation,

$$m_\alpha \frac{d\vec{v_\alpha}}{dt} = q(\vec{E} + \vec{v_\alpha} \times \vec{B}) \tag{3.3}$$

An interesting result of this equation important to the dynamics of filaments is when Eq. (3.3) is boosted to the inertial frame moving with velocity, $\vec{v} = \vec{E} \times \vec{B}/B^2$. Substituting this transformation into Eq. (3.3) yields zero acceleration for the particles. That is, an electric field causes a constant drift velocity of the particles for a particular species, independent of charge, and perpendicular to both $\vec{E}$ and $\vec{B}$. The same mathematical treatment can be applied to an arbitrary force, $\vec{F}$ acting on the particle. Here, the resulting velocity drift is,

$$\vec{v}_{\vec{F}} = \frac{\vec{F} \times \vec{B}}{qB^2} \tag{3.4}$$

which is, again, perpendicular to both $\vec{F}$ and $\vec{B}$ but may now depend on charge. In a toroidal device such as VTF, the magnetic field has the form $\vec{B} = \frac{r_0 B_0}{r}\vec{e}_\phi$ in cylindrical coordinates (r, ϕ, z) where $\vec{e}_\phi$ is the toroidal direction and B_0 is the magnitude of the magnetic field at reference position, r_0. A field of this form introduces a charge-independent effective force due to and proportional to the curvature and gradient of the magnetic field. The independence of the effective force on the charge means that the drift velocities of the ion species and the electrons will oppose with equal magnitude. Separation of charge creates a charge distribution and subsequently, an electric field to oppose the separation and restore an equilibrium. The physical result of this process becomes more illuminated when considering the continuity of this current, i.e. $\nabla \cdot \vec{J} = 0$, throughout the filament structure.

Starting from the MHD equation of motion with an additional arbitrary force density term, $\vec{f}$, mass density, ρ_m, drift velocity, $\vec{v}_{\vec{E}\times\vec{B}} = \vec{E}\times\vec{B}/B^2$, $\vec{b} \equiv \vec{B}/B$, and pressure, p, we have,

$$\rho_m \frac{d}{dt}\left(\frac{\vec{E}\times\vec{B})}{B^2}\right) = -\nabla p + \vec{J}\times\vec{B} + \vec{f} \tag{3.5}$$

Taking $\nabla \cdot \frac{\vec{B}}{B^2}\times$ Eq. (3.5) and noting the following vector quantities and identities for arbitrary vector, $\vec{A}$,

$$\vec{B}\times(\vec{A}\times\vec{B}) = \vec{A}_\perp \tag{3.6}$$

$$\begin{aligned}\vec{\kappa} &= \vec{b}\cdot\nabla\vec{b} \\ &= -\frac{\vec{e}_r}{r} \qquad (curvature)\end{aligned} \tag{3.7}$$

$$\frac{dn}{dt} = \frac{\partial n}{\partial t} + \vec{v}\cdot\nabla n = 0 \quad (continuity) \tag{3.8}$$

where subscripts $\perp$ and $\|$ denote that the direction of the vector is with respect to the direction of the magnetic field, we get the vorticity equation [5],

$$\nabla\cdot\left(\frac{\rho_m}{B^2}\frac{d\vec{E}_\perp}{dt}\right) = \nabla\cdot\vec{J}_\perp + \frac{2}{B}\vec{b}\cdot\left(\vec{\kappa}\times\left[\vec{f}-\nabla p\right]\right) - \frac{\vec{b}}{B}\cdot\left(\nabla\times\vec{f}\right) \tag{3.9}$$

In toroidally symmetic plasma filaments, $\nabla\cdot\vec{E} \approx \nabla\cdot\vec{E}_\perp$ allowing the left hand side to be rewritten as,

$$\begin{aligned}\nabla\cdot\left(\frac{\rho_m}{B^2}\frac{d\vec{E}_\perp}{dt}\right) &\approx \frac{\rho_m}{B^2}\frac{d}{dt}\nabla\cdot\vec{E}_\perp \\ &= \frac{\rho_m}{\epsilon_0 B^2}\frac{d\rho_c}{dt}\end{aligned} \tag{3.10}$$

where ρ_c is the charge density and the first step results from use of the Boussinesque approximation. By (3.10), the left hand side of equation (3.9) is approximately zero via the continuity equation, Eq. (3.8). The vorticity equation shows how a charge density displaced by the current due to internal and external forces establishes

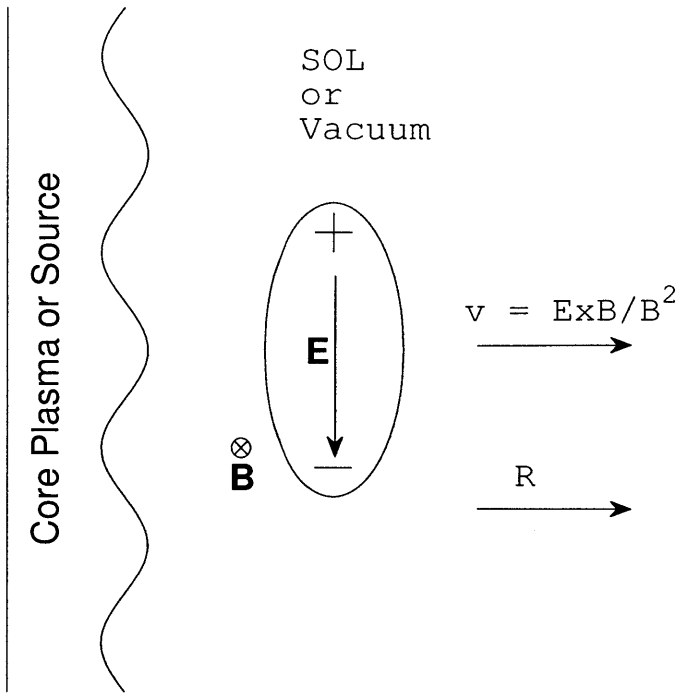

Figure 3-2: Filament Drift and Polarization: A Filament separated from a core plasma or from another source in a magnetic field $\vec{B} \sim \frac{\vec{e}_\phi}{r}$ acquires a polarization field, $\vec{E}$, which drives the radial drift.

the perpendicular electric field. The physical model developed by Krasheninnikov, D'Ippolito, and Myra relates these currents and electric fields to more tangible ideas.

3.2.2 Sources of Drift

Equation (3.9) shows mathematically how different forces acting on the plasma and the pressure will induce internal currents through vorticity and how the charged particles maintain current continuity by closing current loops. The drifts due to forces, $\vec{f}$, form currents in the filament closed by vorticity. With each relevant $\vec{f}$, an electric field forms resulting in an effective drift for the filament. These forces include those due to inherent geometric effects and properties of the plasma as well as external forces.

In any plasma device with a nonuniform magnetic field, the charged particles will

feel an effective force owing to changes in the magnetic field within the motion of the particle about its guiding center. These effective forces derived from and named for the curvature and the gradient in the magnetic field cause drift velocities related to the fields as,

$$\vec{v}_{curv} = -\frac{mv_{\parallel}^2}{qB}\vec{b}\cdot\nabla\vec{b}\times\vec{b} \tag{3.11}$$

$$\vec{v}_{grad} = -\frac{mv_{\perp}^2}{2qB}\nabla \ln B\times\vec{b} \tag{3.12}$$

In VTF, for example, where $\vec{B}\sim\vec{e}_{\phi}/r$, both Eq. (3.11) and Eq. (3.12) are proportional to $\vec{e}_z/q$. That is, the ions will drift upwards and the electrons downwards polarizing the filament with an electric field in the -$\vec{e}_z$ direction. This generates the initial charge-independent radial drift of plasma filaments as depicted in Fig. 3-2. The plasma filaments experience more than just these magnetic geometry forces, which change the final characteristics of the polarization field and thus the radial transport. In [4], a few example forces are applied to the theory just described.

In a partially ionized plasma, a neutral drag force is felt by the propagating filament structure of the form,

$$\vec{f} = -m_i n\nu\vec{v} \tag{3.13}$$

where ν is the collisional requency between the ions and the neutrals. Since the electric field drifts that are in the radial direction dominate the dynamics of the filament, $\vec{v}$ in Eq. (3.13) is usually written as $\vec{E}\times\vec{B}/B^2$. Since the electric field is connected to the structure of the plasma filament, gradients of the electric field drift velocity will have negligible effects within its rest frame. Thus, substituting this term into Eq. (3.9) yields,

$$\vec{b}\cdot\nabla\times\vec{f} = -\frac{m_i}{B}\left(\nu\frac{E}{B}\right)\frac{\partial n}{\partial z} \tag{3.14}$$

The effects and dependence of the neutral drag term on the plasma filament and its properties have been experimentally verified and analyzed by Katz, et al [3]].

A family of forces discussed in [1] yield similar results. These include forces that may be written in the general form of $\vec{f} = mn\vec{g}_{ef}$, where the scale of spatial variations in the effective acceleration, $\vec{g}_{eff}\propto\vec{e}_r$, is much less than that of the background

densities. Such forces add terms to the vorticity equation of the form of Eq. (3.14) where the effective acceleration was $\vec{g}_n = \nu\vec{v} = \nu E/B$, or the term in parentheses in Eq. (3.14). Some other example forces include those of the curvature force, $\vec{g}_{curv} = 2c_s^2/R$; centrifugal force for a rotating plasma column with radius a and angular momentum L_θ, $\vec{g}_{cent} = L_\theta^2/a^3$; and thermal expansion of a filament of length $L_\parallel$ against an angled limiter, $\vec{g}_{te} = 2\left(c_s^2/L_\parallel\right)\cot\theta$. The charge independence of each of these forces has the same effect as the curvature and gradient forces on the poloidal currents and electric field. Forces such as the neutral drag with negative terms of vorticity reduce the electric field by lowering the polarizing current and thus the current available for closing the loop. The conductive properties of the plasma and relationship of these system forces to circuit components led to a circuit model to explain the problem of filament dynamics.

3.2.3 Circuit Model and Hypotheses

Krasheninnikov, Myra, and D'Ippolito present a model detailing their circuit model of filament polarization and drift [1]. In this circuit model, the polarized filament acts as a current source. Since $\nabla \cdot \vec{J} = 0$ in a quasineutral plasma, electric fields are set up across the sheath resistor and the current due to the resistivity of parallel and perpendicular flow to drain the current. The equilibrium polarization of the filament establishes the potential drop across the parallel circuit model as seen in Fig. 3-3a.

This experiment alters the model by cutting off the circuit model with two identical voltage sources on either side of the filament. The ammended circuit model is shown in Fig. 3-3b. A sheath forms at the boundaries where current is pulled in and out of the limiter which gives rise to the impedance associated with it. In the modified circuit model with the limiters included, the limiter voltage source establishes an independent electric field. The limiter, therefore, acts as an additional independent source or drain of current through its sheath resistance.

When the field generated by the plates equals the natural field generated by the drift mechanisms, the total current drawn by the limiter plates should cancel and the

filament should therefore be behave as though the limiters were not there. This blind spot serves as the reference potential from which effects are measured. When the potential drop across the filament where it contacts the limiter exceeds that of the reference potential, the field across the filament increases enhancing the polarization and the effective radial drift. Likewise, when the potential drop across the limiter and the sheaths is negative, the electric field felt by the filament is reduced and so is the radial drift. In these experiments, we expect to see the changes in radial propagation of the filament to the extreme case where the filament may drift back towards the source near the inner wall.

The circuit model offers a simplified interpretation of the complexity of filament dynamics and the effects of this or future experiments with filaments and the effect of sheath interactions. The circuit model averages the electrical dynamics within the filament structure yielding a simple solution to their effects. Replacing all of the characteristic properties with their lumped circuit component analogs such as $\eta_\perp \rightarrow R_\perp$, $J_\perp \rightarrow I_\perp$, etc. yields the equation for the perpendicular voltage drop as a function of polarization current and the limiter voltage drop,

$$V_\perp = \frac{R_\perp}{Z_{tot}} \left[V_{lim} + I_p \left(Z_{tot} - R_\perp \right) \right], \tag{3.15}$$

where $Z_{tot} = \sum R_i$. To relate this to the magnitude of the radial propagation of the filament, we note that $V_{lim} \approx E_{lim}\delta_z$, $v_r = E_\perp/B = V_\perp/(\delta_z B)$ and $[I_\perp, I_p] \approx [J_\perp, J_p] \times L_\parallel \delta_r$ where δ_z and δ_r are the size of the filament in the z- and r-directions, respectively, and $L_\parallel$ is the length of the filament between limiters. Substituting these relationships into Eq. (3.15) yields our estimate for the expected filament velocity, v_{fil}, as a function of limiter electric field,

$$v_{fil} = -\frac{\eta_\perp}{Z_{tot} B} \left(\frac{\delta_z}{L_\parallel \delta_r} E_{lim} - (Z_{tot} - \frac{\eta_\perp \delta_z}{L_\parallel \delta_r}) J_p \right). \tag{3.16}$$

From Eq. (3.16), we see the expected linear dependence on the field established by the limiter along the terminal ends of the filaments.

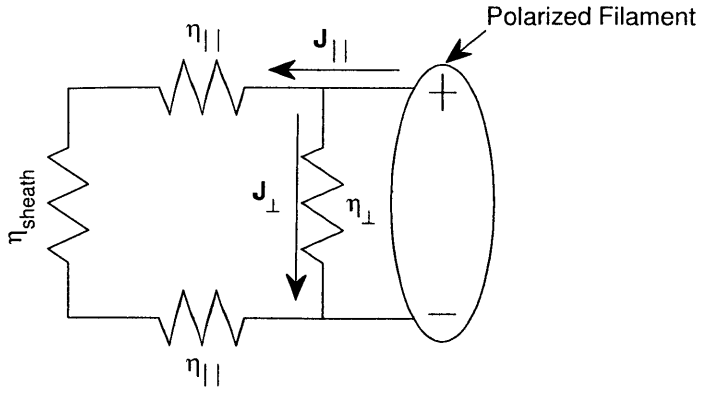

(a) Krasheninnikov, Myra, and D'Ippolito

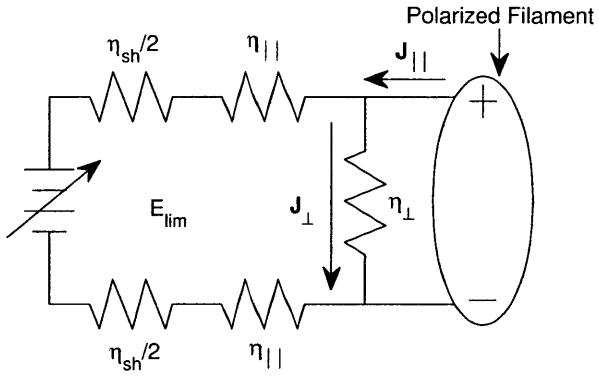

(b) Experiment

Figure 3-3: Circuit Model: The circuit model, (a), as proposed by Krasheninnikov, Myra, and D'Ippolito to show the current paths and closure schemes within a sheath-connected, polarized filament. The path resistors are defined by the associated resistivities: $\eta_{||}$ and $\eta_{\perp}$ are the plasma resistivities along the parallel and perpendicular paths with respect to the magnetic field. The circuit model, (b), as given for this experiment with the inclusion of a variable power source.

Chapter 4

Results

As stated in chapters 2 and 3, the primary diagnostic tools for the filament experiments are 4 Langmuir arrays and the limiters. One configuration producing long filaments ($L_{||} \sim 6$ m) via ECRH uses all 6 arrays in diagnosing the plasma. The other configuration uses 1 of the hanging Langmuir arrays and both limiters for short ~1 m-long plasmas from the argon gun injection system. The two configurations offer a look at filaments of different parameters to corroborate or reveal consistencies or inconsistencies seen in one another.

Two sets of digitizers controlled the time resolution of the diagnostics. The three hanging arrays described in section 2.4.1 and the limiters have data digitized at 500 kHz or with 2μs resolution. The side-loaded array's data is digitized at 2 MHz or with .5μs resolution. The experiment is controlled by LabView^{TM} starting and ending with the digitizers switching on then off with apparatuses activity determined in reference to these times. For the fast digitizers in a 10 ms experiment, 20000 data points are taken for each individual Langmuir probe signal (5000 for the slower digitizers). At time points of ~10000 (~2500), the microwaves or the plasma gun initiate creating a plasma that lasts approximately 1 ms or 1000 (250) data points in time. Each configuration has 3 regions of different activity (of which only one has meaningful data) during each experimental run referred to as a shot.

4.1 Data Handling and Regions of Interest

Prior to and encompassing plasma generation is initialization where the diagnostic signals pick up electrical signals from the start-up sequence. The third region begins when the plasma reaches the outer wall of the chamber or dissipates to the point where it can no longer be resolved by diagnostics. The remaining time comprising the second region is when the filament is in view of the diagnostics. Due to overlap with the first and third the regions, only a portion of this time represents useable data. For instance, calculations such as center of mass require the entire filament to be within range of the Langmuir probes as well as the limiters which do not cover the same cross-sectional area. These limitations exclude all times up to and just passed shut down of the source. The limiters act to dissipate the filament and shorten the time in which the filament is resolvable, especially in the gun configuration. From the original 20000 (or 5000 for the slower digitizers), up to a thousand (or a few hundred) remain relatively untainted by the temporal and spatial boundaries stated above. To determine the period of time containing relevant and reliable data, movies rendered in Matlab reveal the times when the plasma exhibits filamentary structure. Frames of these movies are shown as example in Fig. 4-1. Times chosen using the movies are a means of reducing error in position and velocity by visual recognition of error inducing effects and non-physically relevant signals. In this now determined time span, the spatial characteristics of the filament and current drawn by the limiter are used to calculate velocities and resistances applicable to the circuit model in section 3.2.3.

4.2 Filament Position, Speed, and Error Reduction

The main characteristic of interest in dynamic flow of filaments is the speed determined by the motion of the density measurements. Since VTF is set up with digitizers of known time steps between data points, similarly accurate characteriza-

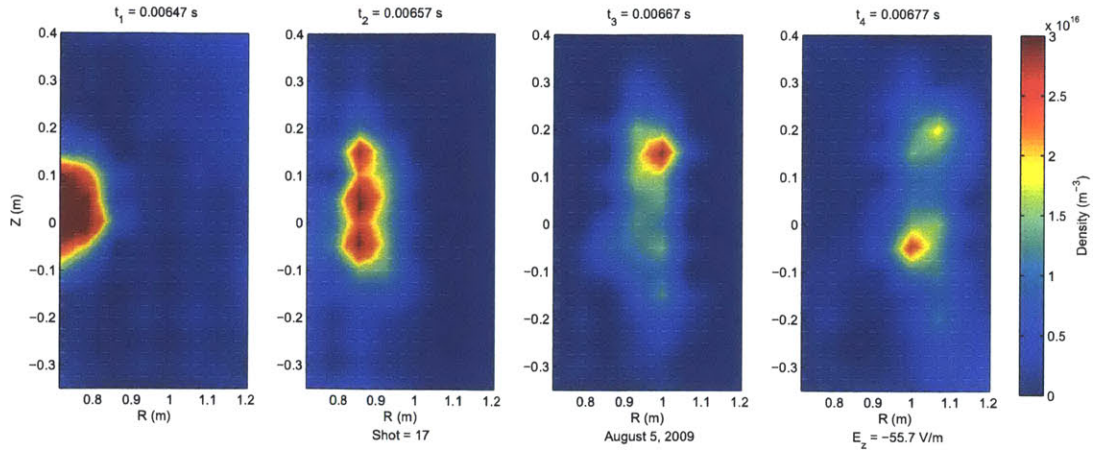

(a) ECRH

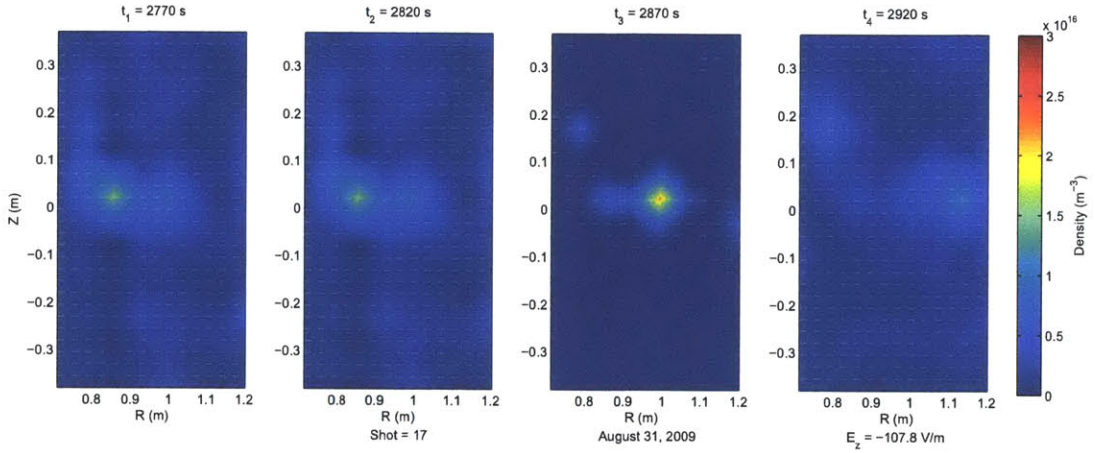

(b) Gun

Figure 4-1: Filament Propagation: Four time frames of filament propagation as depicted by the Langmuir array data rendered using Matlab.

tion of the position of the filament was very important. In this experiment, position evolution and thus velocity were computed in a number of different ways depending on the configuration and limitations set forth by the boundary interactions described previously.

In the configuration producing long filaments by ECRH, a center of mass calculation along the radial direction provided the simplest and most effective means for determining the radial movement. With the particle density as the weighting function, w, and radial position, r, the center of mass for a shot was calculated for each relevant time point as,

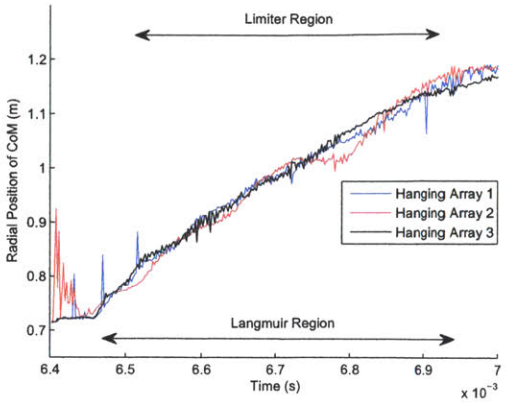

(a) Center of Mass

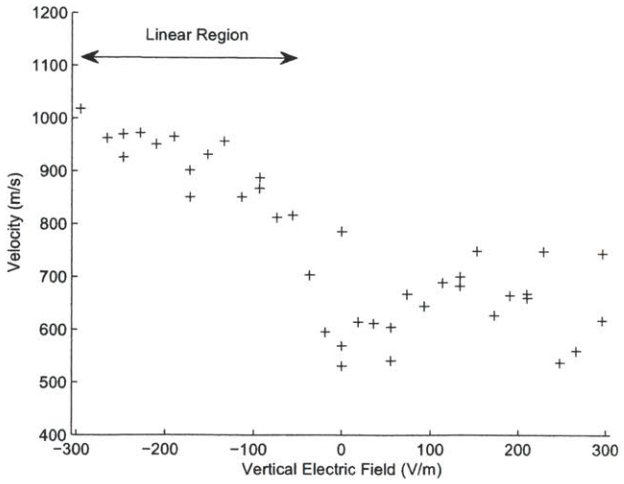

(b) Velocity

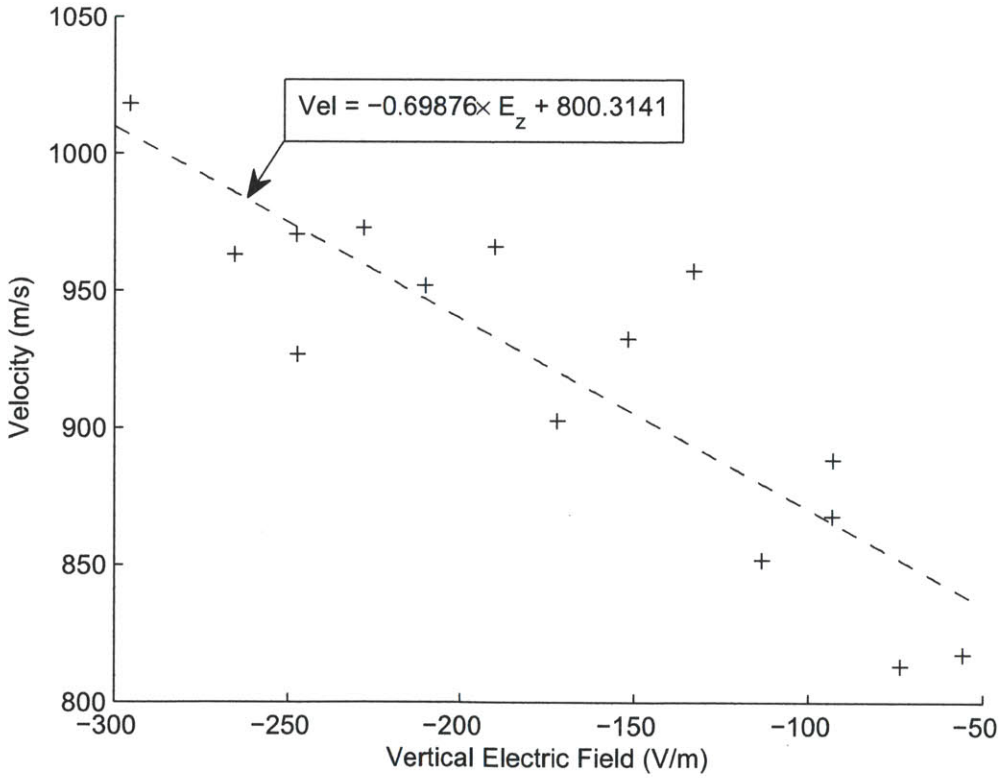

(c) Linear Region

Figure 4-2: Velocity: The filament velocity data (b) as a function of the vertical electric field of the limiter as derived from center of mass (a) calculations. Figure (c) separates and shows the trend line for the linear region.

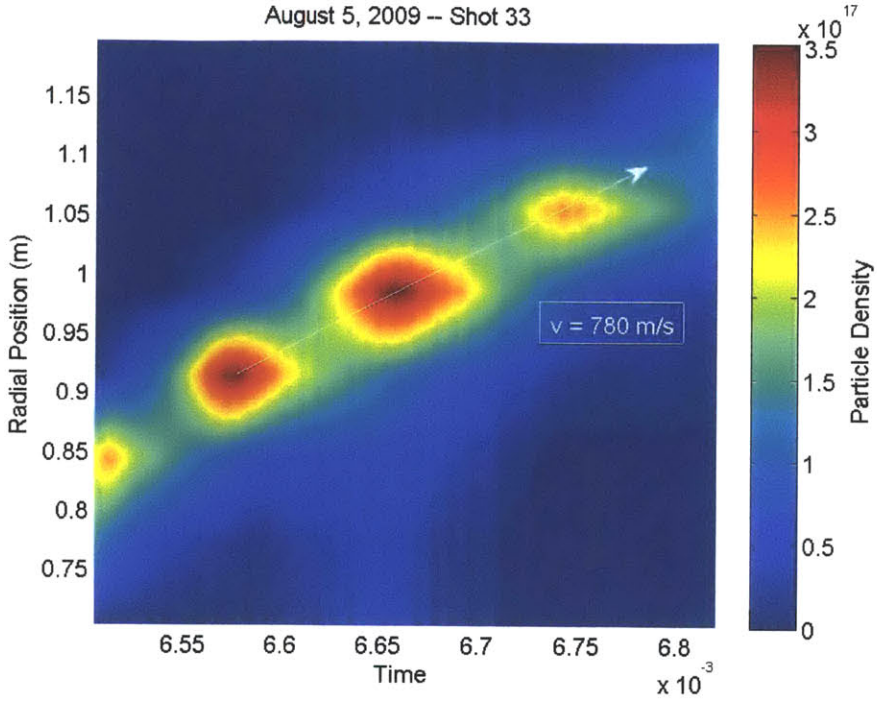

(a) ECRH

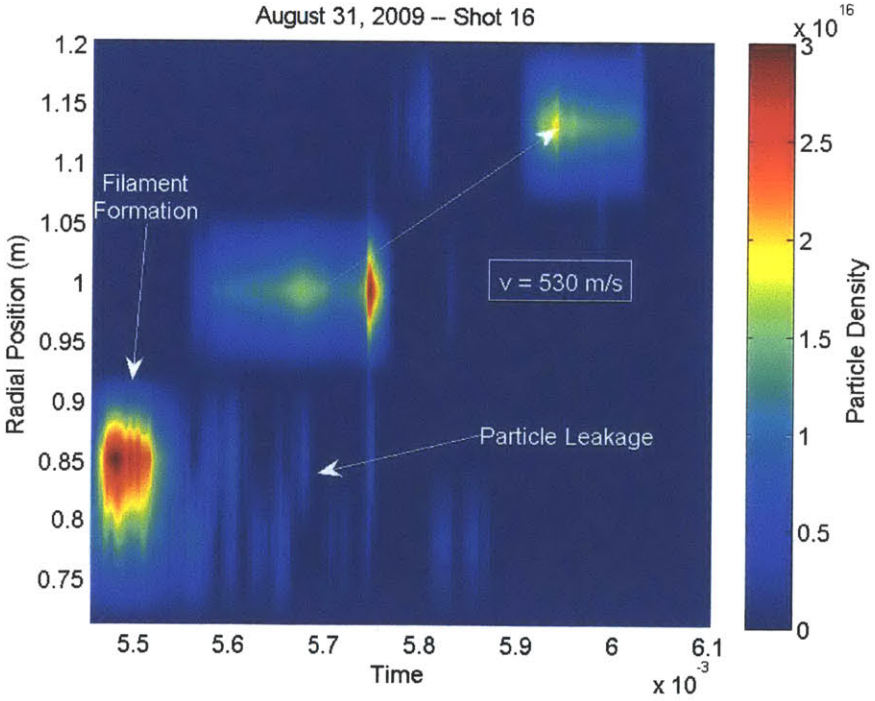

(b) Gun

Figure 4-3: Time of Flight: R position moments of the particle density versus and smoothed in time.

$$\bar{r} = \frac{\sum_{i,j} w_{ij} r_{ij}}{\sum_{i,j} w_{ij}} \tag{4.1}$$

where (i,j) are the (x,y) grid of the Langmuir arrays in biased mode. The average time derivative over the relative time period of the results of Eq. (4.1) determined the velocity of the filament reported by each Langmuir array. Examples of a plot of center of mass as a function of time and a summary of the resulting velocity calculations are shown in Fig. 4-2. Tracking the center of mass is a robust and simple way of determining the velocity but signal noise has a tendency to more significantly alter the calculated center of mass. For instance fluctuations that occur at the vessel wall when the filament is near the inner wall have a large enough weight in Eq. (4.1) to significantly throw off the calculated center of mass from the real one. To combat this error, the signals are filtered by their magnitude relative to that of a typical filament.

In a typical shot of long plasma filaments, the charged particle density reaches just above 3 $\times 10^{16} m^{-3}$ at its peak. The poloidal scaling of the filament ($\sim$ 10cm) is large enough that it spans multiple probe tips in the radial and vertical direction. Thus, the peak density detected from any of the probes for a given time does not drop below 1 $\times 10^{16} m^{-3}$ until the filament has dissipated beyond being a coherent structure. Knowing this fact, reducing the noise for center of mass calculation was accomplished by determining a cutoff density and rejecting signals corresponding to values too low to be part of the filament. Random noise generally could not produce statistically significant particle densities. Therefore, the cutoff density was chosen as 1/10th of the peak density measured, typically $\sim 3 \times 10^{15} m^{-3}$. To verify that the filament was unaffected by the cutoff, plots generated of the filament at different time points were compared to the unaltered data. The method of cutting out noise worked well but only under the condition that the filament was large enough and the noise did not reach the magnitude of the actual filament signals which occurred only sparsely.

When generating a plasma in the argon gun configuration, a few issues presented

themselves preventing use of the center of mass method. First off, the plasma filaments were miniscule in comparison; with poloidal dimensions of generally less than $10cm$. As in the large filament scenario, the peak density may be lost as it travels in between the individual Langmuir probes. The large filaments have a large enough scale to resolve essentially the same image of a filament throughout the experiment. With spatial scales on the order of that of the smaller filaments $\lesssim$ 10 cm, however, comparatively more of the image is lost between probe tips. The edges of the filaments still measured by the probes might resemble noise, which the center of mass calculation would ignorantly remove. Other center of mass error inducing properties, however, also gave cause for using a different positioning method.

As is a tendency with other plasma injection systems similar to VTF's argon gun [6], the source leaks plasma particles after the initial arcing and plasma production pulse has ended. The leakage could be due to interactions with the gun structure slowing down already low energy particles or residual voltages ionizing local neutrals. In any case, a low but nontrivial amount of plasma particles appear to be born after the filament creation and propagation have begun. The particle density plots show this as small blob of plasma forming near the edge of limiters as seen by the Langmuir arrays. Build-up and lack of further propagation suggests that these particles either dissipate energy quickly and recombine or are absorbed into the limiters. The method used to circumvent these error inducing effects is based on a time of flight measurement.

First, all of the data from the probes from the inner wall to where the charge build-up occurs were deemed contaminated and not used. Then, for each time point, the data was collapsed along the vertical direction since the radial propagation is of more interest than vertical, which was generally negligible in any case. The collapse means that data for each radial position was a sum of all probe signals at that radial position. From here, the maximum summed particle density was plotted and tracked. That is, at a given radial position, the first passage of a maximum on an order greater than $2 \times 10^{16} m^{-3}$ was noted as shown in Fig. 4-3. It was important to take data on the first maximum for a given radial position to avoid any possible propagation of the

leaked charged particles after the filament had passed. The averaged velocity would simply require dividing the distance between each probe by the time recorded for the initial maximum.

4.3 Sheath Resistance

The resistance of the sheath in the circuit model of Fig. 3-3 was measured by driving a current straight through the plasma from one limiter to the next. For this to work, the limiters were setup as a cathode and an anode each at one particular voltage. The uniform voltage on each limiter and across the filament is the equivalent of superimposing a voltage drop across the model of Fig. 3-3a along the axis of the filament. The dynamics of the filament were relatively unaffected due to the induced flows being parallel to the magnetic field. As the filament moves across the frame of the limiter, the peak currents in one and out of the other determined the effective resistances. Figures 4-4 to 4-6 give examples of the current distributions and total currents collected by the limiters while driving currents through the resistive sheaths. As the filament propagated radially, the current collected at one point along the inner side of the limiter and then quickly moved across to the other side of the limiter. The time at and speed with which this happened did not seem to correlate to the position and speed of the blob. The change did occur near the maximums in current collection (see Fig. 4-4a and when the filament was fully developed and in view of the limiter. For this reason, the current readings were taken with averages near the peak during this transition that is more visually depicted in Fig. 4-4b with a summary of the results in Fig. 4-6 for the data retrieved in the ECRH and gun configurations. The resulting calculated resistances are $\sim$ 17 kΩ and 300Ω for ECRH and gun configurations, respectively.

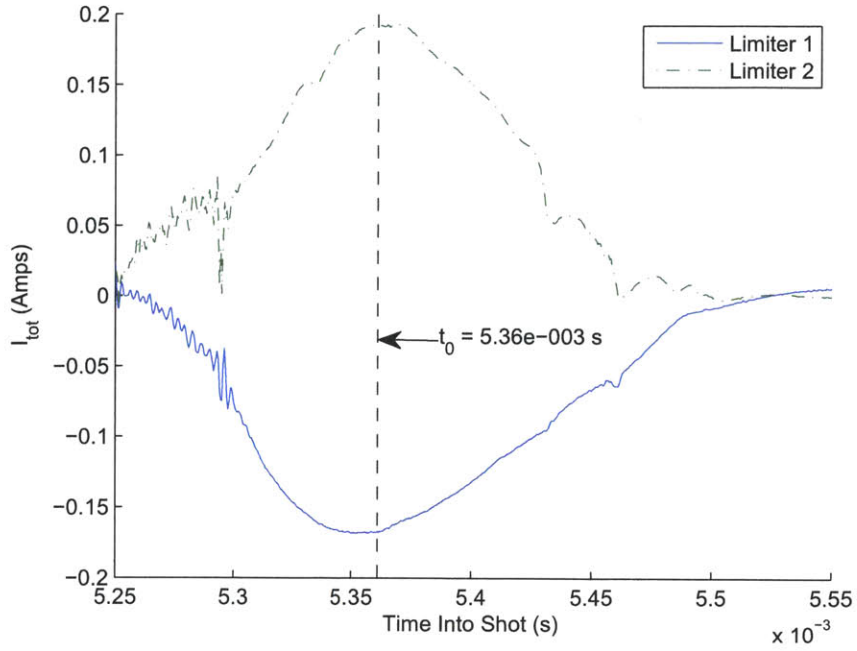

(a) Total

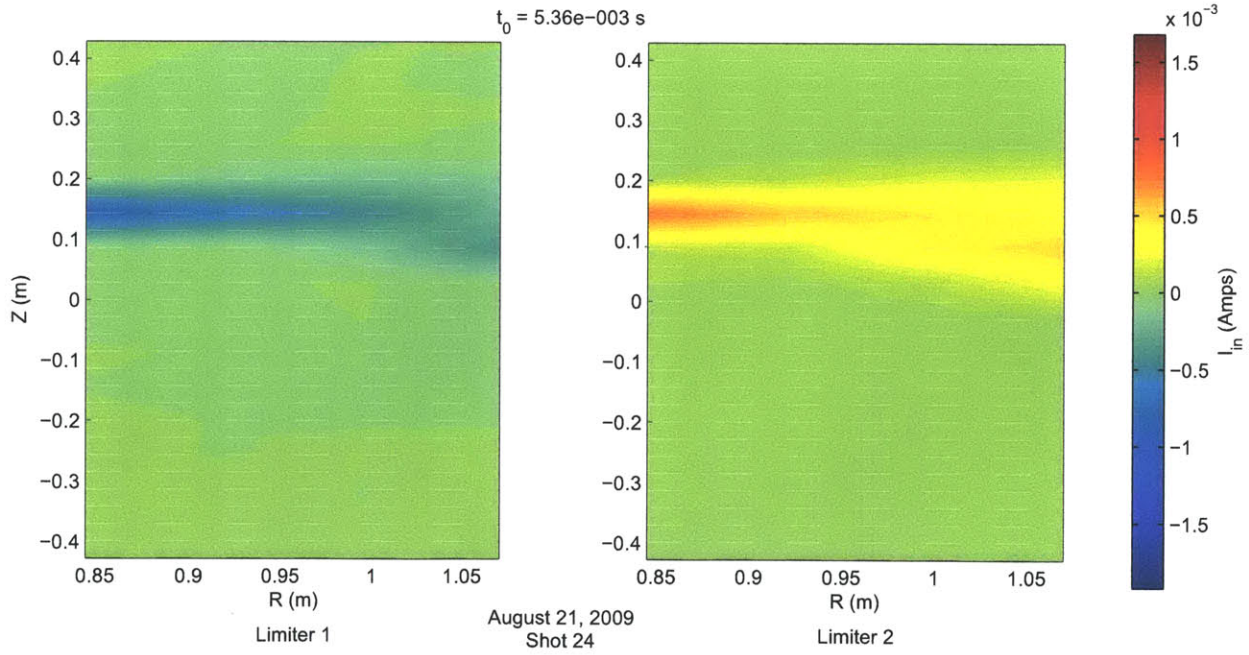

(b) Distribution

Figure 4-4: Negative Voltage Current Drive: An example plot (a) of the total currents into and out of the limiters driven by a potential difference below the system ground. The associated current distributions (b) across the limiters at time, $t_0 = 5.36 \times 10^{-3}$s.

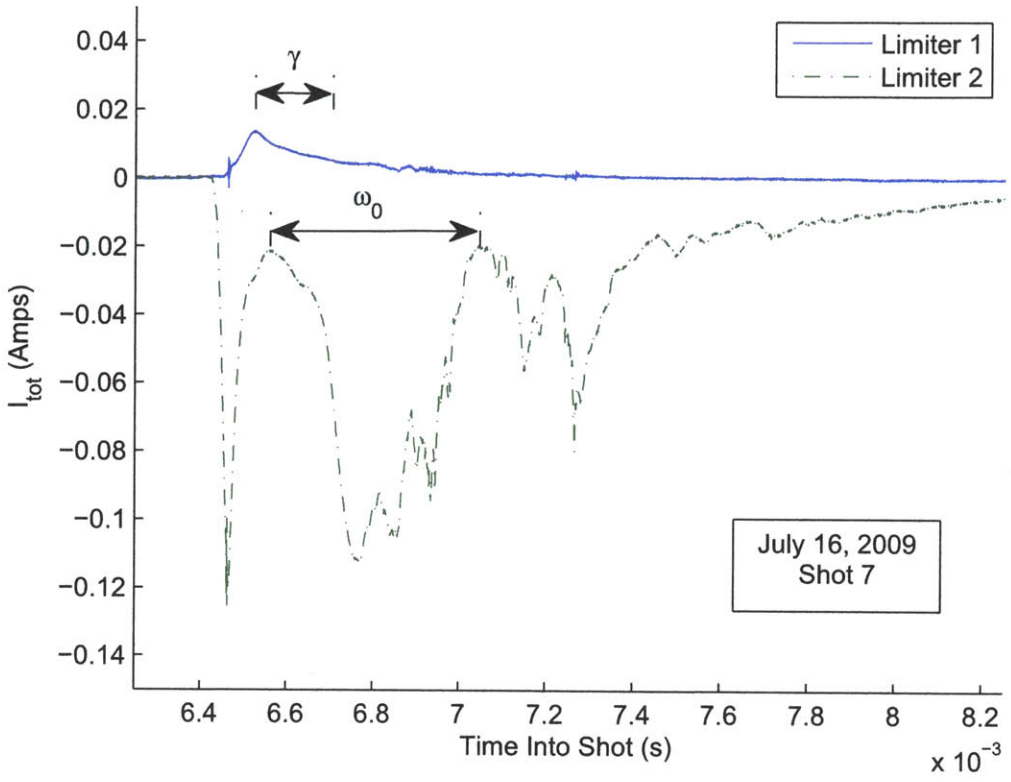

Figure 4-5: Positve Voltage Current Drive: An example plot of the current into and out of the limiters driven by a potential difference above the system ground. In the current data, a long-lived oscillating and attenuating transient is seen with approximate frequency and decay of $\gamma = 2.8 \times 10^{-3} s^{-1}$ and $\omega_0 = 6.5 \times 10^{-3} s^{-1}$.

4.4 Potential

Even though the data on the plasma potential as measured by the Langmuir arrays was deemed unreliable, the qualitative features of polarization associated with the potential and, as we found, the current into the limiters have interesting characteristics. For example, a newly created filament gains an initial polarization, but when it contacts a limiter set up to slow it down, the still frames from the movies show the polarization of the filament and its current flipping direction. In Fig. 4-7, still frames of filament potential and parallel current from movies of different applied electric fields are shown. For a more quantitative perspective of the current distributions shown in Fig. 4-7, the data of the current was split and treated separately in terms of both the current in and out of the limiters. Figures 4-8 and 4-9 summarize

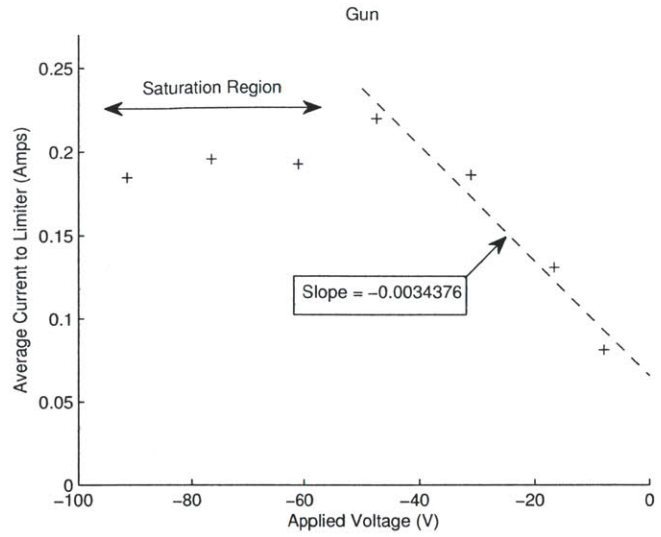

(a) Gun

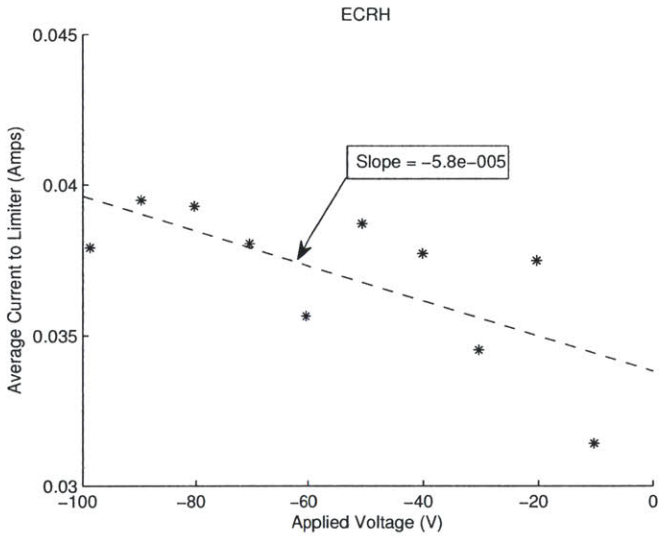

(b) ECRH

Figure 4-6: Driven Current: Plots of the average current driven between the biased limiters: (a) is the data for filaments produced by the argon gun while (b) is that of the ECRH-generated filaments.

the results of that analysis.

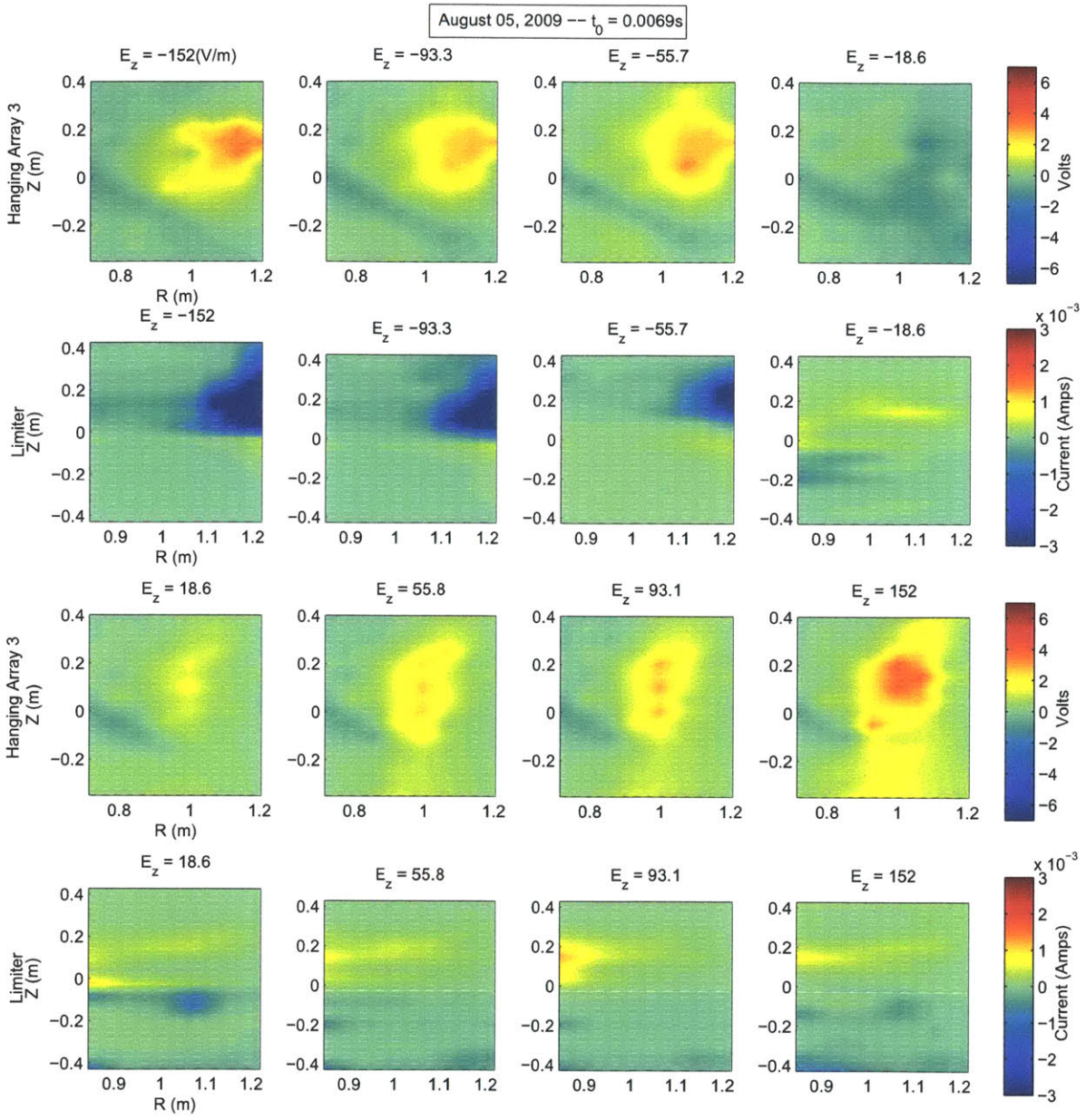

Figure 4-7: Parallel Current Switch: Time frames from shots with different limiter electric fields. The first and third rows show the potential structure of the filament as seen by a Langmuir array while the second and fourth show the parallel current seen by a limiter.

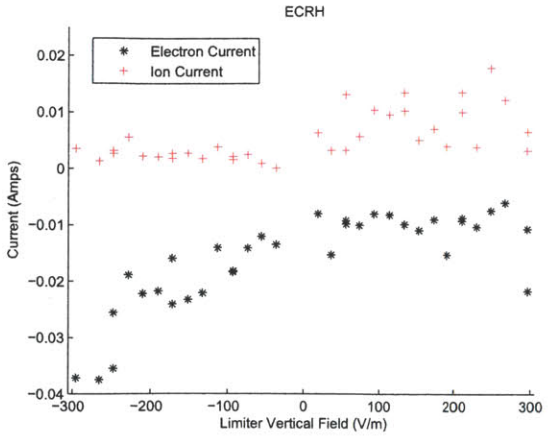

(a) ECRH

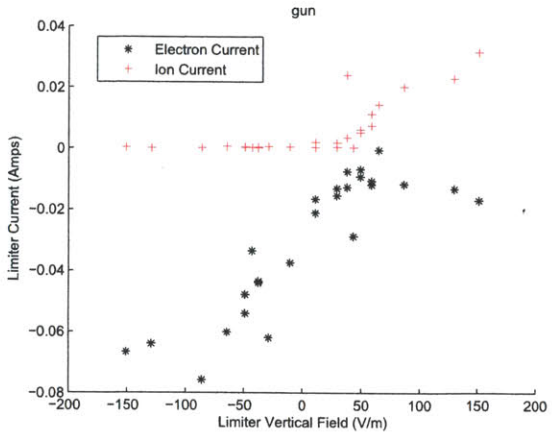

(b) Gun

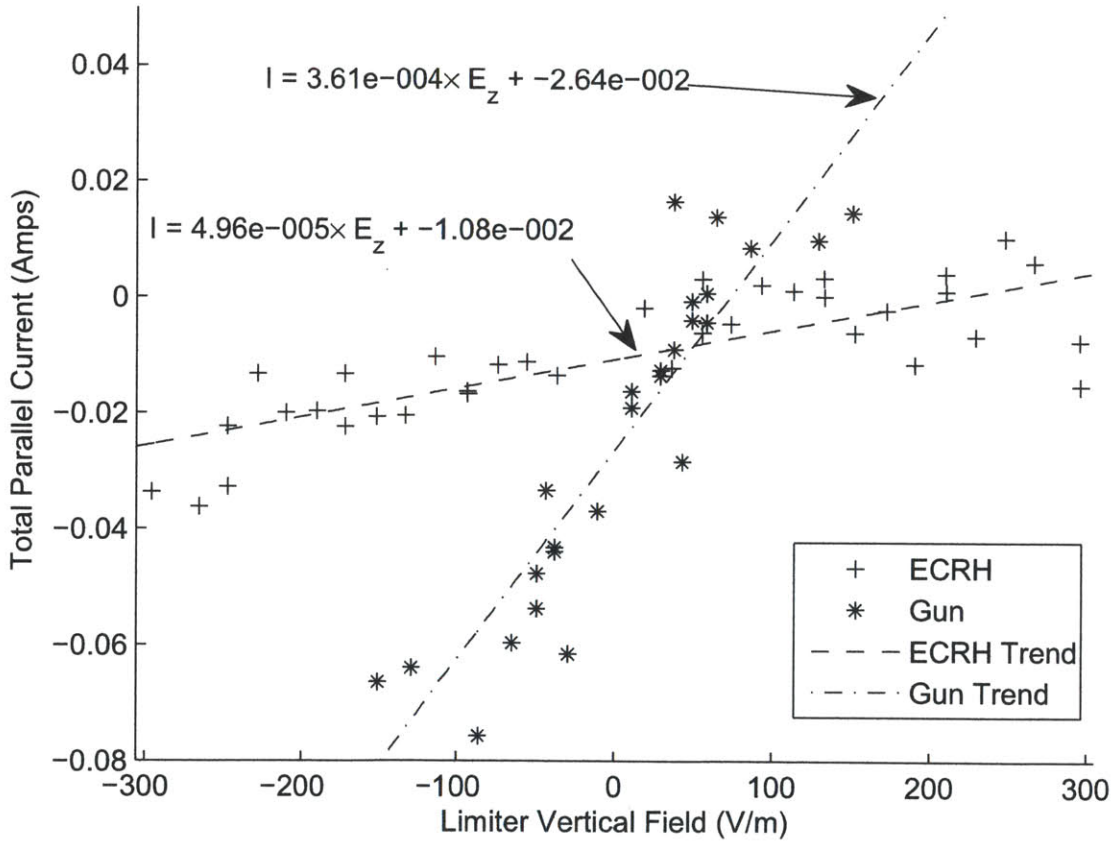

(c) Total

Figure 4-8: Current Versus Electric Field: Plots of the average ion and electron currents for (a) ECRH; (b) gun; and (c) total as measured by the limiters versus the electric field created across it for long ("ECRH") and short ("gun") filaments. Between (a) and (b), we see that current collection by the limiter dominates for positive electric fields and current emission dominates for negative electric fields, i.e. a switch occurs near-zero field.

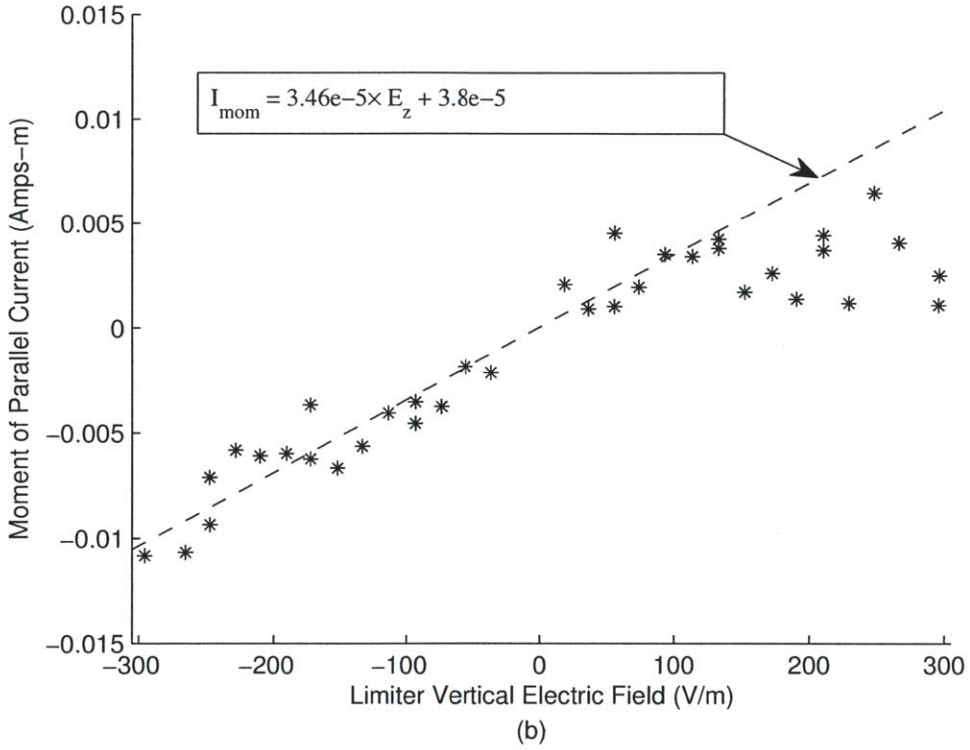

Figure 4-9: Current Collection Moment: A plot of the moment of the parallel current as seen by the limiter from ECRH data.

Chapter 5

Discussion

5.1 Radial Propagation

The center of mass propagation of filaments in the ECRH configuration proved very successful and reliable. Figure 4-2a gives an example of the center of mass of a filament over time as measured by the three hanging Langmuir arrays. Before the filament is produced, the random signal fluctuations for times less than 6.5 ms dominate Eq. (4.1) causing wild fluctuations. These fluctuations carry on as the minor errors in the curve for times where the filament is in view of the Langmuir probe tips. The larger frequency sinusoidal fluctuations in each of the curves arise from the filaments, or at least their peak density regions, 'disappearing' into the space between individual Langmuir probe tips. The other significant feature of the center of mass versus time curves were the changes that occur as the filament transitions from a purely toroidally symmetric filament to the sheath limited regime. That is, the nature of the filament changes, explaining the non-linearity, during the time in which the filament is in view of the Langmuir probes and not the limiters. Prior to contact with the limiter, the filament follows a model similar to Fig. 3-3a without the sheath resistance component. Such a filament would have a significantly larger $\vec{J}_{\perp}$ and thus a larger E×B drift. Thus the final velocity averages as depicted in Fig. 4-2b are comprised of the average time derivative of the curve in the limiter region for the three hanging arrays and the side-loaded Langmuir array.

For at least a region of the negative vertical electric fields, the velocity data shows a linear trend with the vertical electric field set up by the limiters. In this region, the change in velocity varies approximately as -.69 times the relative change in the limiter electric field. The hypothesis presented in section 3.2.3 exactly predicts a negative linear relationship. With the calculated parallel resistances for the filaments produced by ECRH, the circuit model's linear coefficient, by Eq. (3.16), is approximately -.19.

Surprising about Fig. 4-2b however, is the lack of correlation between velocity near and above a zero electric field. Not much in the initial density data from the Langmuir probes suggested any reason for the breakdown and the simple circuit model does not suggest any complex nonlinearity for any specific region of electric field along the limiter. The model, however, does suggest the characteristic electric field in which a change in behavior is expected and that is around the reference electric field.

At the reference electric field which matches that which would develop in the toroidally symmetric filament, i.e. one not subject to sheath connectivity effects, no current should cross into the limiters. All of the current from drift mechanisms will drain back through the perpendicular channel and the filament would behave as if it were not contacting the limiter. This electric field would be slightly negative. Conveniently enough, the data's linear region begins to break down at a negative electric field suggesting some complicated behavior when the limiter switches from driving a filament faster to impeding its 'natural' propagation. To determine the validity of this speculation, we look to characterize the peculiar switching of the parallel currents as seen by the limiters.

5.2 Currents

As suggested by Fig. 4-7, the relative positions of current collection and emission are variable as well. Variable to the point that the relative vertical position of positive and negative parallel currents switch about some negative value for the limiter electric field. Using a 'center of current' calculation with $w_{ij} = I_{ij}$ and $r_{ij} \rightarrow z_{ij}$ in Eq. (4.1), a dipole-like term was calculated. The strength of this parallel current moment equalled

the vertical displacement between these centers of current times the current intensity. Theory and the model suggest that the strength of this dipole would correspond to the electric fields centered about the reference field where the moment should be zero. As Fig. 4-9 shows, a clear linear correlation does in fact exist with some disparity developing for very large positive vertical electric fields. For very negative electric fields, the current leaves the top of the limiter and the filament, and then crosses the magnetic field establishing a larger filament electric field. Similarly, the parallel currents for larger positive limiter electric fields show current leaving the bottom of the limiter and traveling across the magnetic field decreasing the filament electric field established by its inherent currents. However, the point at which this parallel current moment equalled zero did not correspond to as negative of an electric field as both Figs. 4-2b and 4-7 suggest. The moment seems to switch slightly less than but very close to zero limiter electric field. Not enough data was collected near-zero electric field to show where the actual switch in the moment occurs, but looking at the current in and out separately suggests a possible reason for the discrepancy in determination of the reference electric field.

For current continuity, the individual currents in and out of the limiters should be equal in magnitude. The data summarized in Figures 4-8a and 4-8b show an obvious disparity between these parallel currents. In both the gun and ECRH configurations, only about half of the current data follows the linear trend as expected while the other data appears to be constant and much closer to 0. This suggests that half of the current is lost to some unknown mechanism. For negative electric fields when the current moment is negative, the current is net negative and vice versa for positive electric fields and current moment. Once again, for larger positive electric fields, fluctuations occurred. The transition, too, for this effect of current disappearance was near the 0 electric field point, but in both cases, the dominating current was the one located at the larger z-position. The only path to ground for the charged particles significant enough to cause such a disparity would be to the chamber walls of VTF. The linear region in the velocity data of Fig. 4-2b suggests that the currents still cross the magnetic field as expected but are lost to the walls afterwards for a strong enough

negative limiter electric field. For weak or strongly positive limiter fields, the path becomes interrupted by these wall or other interactions resulting in the complicated behavior for the nonlinear regions of Fig. 4-2b. Evidence of significant interactions dependent on the bias potential is shown as well in the currents driven to measure sheath resistance when biased positive with respect to ground (see Figs. 4-4a and 4-5). Unfortunately, no diagnostic in the experimental setup is capable of showing the level of impact of the wall interactions on these studies with certainty.

5.3 Errors and Unexplored Events

During the course of this investigation, a portion of the data was deemed unusable for the purposes of characterizing the radial propagation effects due to the limiters. The data showed an inconsistency and errors of an extreme nature between the ECRH and gun configurations or were beyond the scope and time frame of the experiments to explore in more depth. Examples of the former include the saturation of currents into the limiter for negative bias and vertical filament propagation while examples of the latter include the effects of filament length and pressure on the resistance, velocity, and current measurements.

5.3.1 Density Errors

The average velocities of the four probe arrays showed good correlation with standard errors of the velocity measurements bein typically less than 1/10th of the magnitude. The time of flight calculations proved difficult to handle even with noting the errors due to particle leakage from the gun. Enough signal noise was present in the density measurements that the standard error on many of the velocity measurements matched the magnitude of the measurement. Between that and the current saturation seen in Fig. 4-6a, the density data for gun-produced filaments was not used in the velocity characterization of Fig. 4-2b and 4-2c.

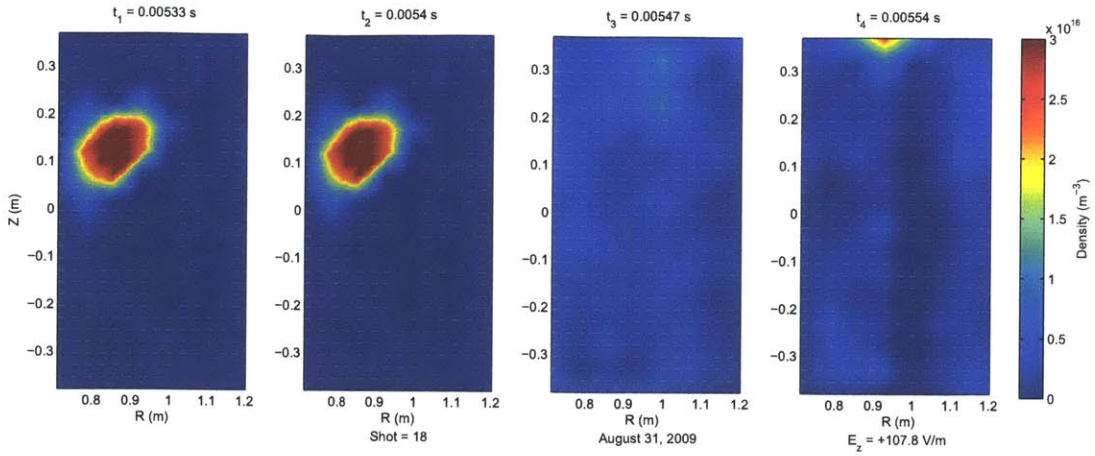

Figure 5-1: Vertical Propagation: An event of vertical filament propagation in an argon gun generated plasma filament.

5.3.2 Vertical Propagation

At large positive limiter fields, the plots of particle density distribution from the Langmuir arrays over time showed evidence of a nontrivial vertical filament propagation shown in Fig. 5-1. Such a flow would require an electric field generated in the radial direction for the appropriate E×B description. A potential source of radial electric field would be through a connection between the filament and the outer (or inner) wall. The errors associated with the floating mode of the Langmuir probes did not allow for appropriate measurements to be taken to definitively resolve the existence of such a field nor confirm the wall as such a source.

5.3.3 Filament Length and Pressure

In the experimental configurations used, the effects on filament propagation were measured for only two different filament lengths: 6 meters and 1 meter. Drift theories suggest that a number of the drift sources have a dependence on the length of the plasma filaments [1, 4]. With only two filament lengths investigated, the effects of filament length are not very clearly shown in any of the data and would require further investigation. As is more clearly evident in the differences between the data collected in the ECRH configuration versus the gun configuration, other parameters besides the field produced by the limiters play a huge role in the resulting dynamical situation

and in particular, the pressure.

A significant difference between the plasma environment for ECRH sourcing versus use of the argon gun is the neutral or vacuum pressure in which the filaments are created. As explained in the experimental setup, the neutral pressures were vastly different due to the way in which the modes create the plasma. The two setups use neutral pressures of almost two orders of magnitude different from one another. In Ref. [3] the velocity parameters were shown to be inversely proportional to the neutral pressure for a toroidally symmetric filament. In this experiment though with a sheath connected filament, the pressure relationships seem to be much more complicated than inverse proportionality and other effects such as current saturation must be accounted for but are for the moment beyond the capabilities of the experiment conducted for this thesis.

Chapter 6

Summary and Conclusions

The experiments of this thesis were designed to investigate the current closure models for filament propagation developed by Sergei Krasheninnikov, et al [1] and gain insight into the fundamental dynamics of filaments in the presence of a limiter. The experiment applied two independent plasma source configurations and diagnosed by 2 limiter arrays and 1 to 4 arrays of Langmuir probes depending on the positioning of the limiters. Limiter construction allowed for the creation of electric fields along the structure by separating the conductive 'wall' into uniform sections electrical independent and capable of carrying a bias potential. This thesis presents the theory, results, and interpretation of the data from these experiments on limited filament dynamics.

In one configuration, long plasma filaments were created by electron cyclotron resonance heating via a solenoid on the inner wall of VTF and a klystron microwave source. This plasma employed all four Langmuir arrays to measure the plasma density as it moved radially through VTF's vacuum chamber and the limiters $\sim 360^o$ apart. In the other configuration with plasma produces by an electrical breakdown of Argon gas injection (the Argon plasma gun), the density measurements were made by a single suspended Langmuir array with the limiters positioned approximately a meter apart. Center of mass and time of flight calculations using the measured density determined the speed at which the filaments propagated radially. Set up of the diagnostics allowed for an easy determination of the sheath resistances in both configurations by driving

current through a potential difference along the filament and between the two limiters. Measurements of the current collected by the limiters helped to verify observations made using the Langmuir arrays.

The radial speed of the filament increased linearly as expected for large, negative electric fields produced along the limiters as described in section 3.2.3 though with a different coefficient. For weak fields and strongly positive electric fields, however, the data was distorted and no trends could be applied to the data when a slowing of the filament propagation was expected. The suggested source for the discrepancies is given as complicated interactions with the wall dependent on the location of the parallel currents and the limiter bias potentials relative to the wall. The evidence for this is in the data for current collected by the limiter where the currents in and out were expected to match but instead a nontrivial amount of current was 'missing' but still affecting the speed of the filament. A number of other events beyond the scope of this thesis were observed with implications of potential effects on radial propagation including filament length, environmental conditions such as neutral pressure, current saturation, vertical propagation, and an unknown attenuating mode that appears with potentials positive relative to ground.

This thesis successfully showed that the constructed limiter could manipulate the current paths within the filament and thus the dynamics of induced radial propagation. However, the largely nonlinear trends in effect of the limiters proved the ineffectiveness of assigning a linear resistance to the parallel paths in the circuit model. The effective resistance parallel to the magnetic field depended greatly on conditions other than simply the presence of a sheath at the limiter. Studying filament propagation is a complicated endeavor with a myriad of interactions to consider and diagnose. Nevertheless, the need for further understanding of their nature is ever present as humanity's need for a well-confined plasma for fusion purposes grows.

Bibliography

[1] S.I. Krasheninnikov, D.A. D'Ippolito, and J.R. Myra, *Jounal of Plasma Physics.* **74**, p. 5 pps. 679-717(2008)

[2] M. Umansky, S.I. Krasheninnikov, B. LaBombard, and J.L. Terry, *Physics of Plasmas*, **5**, 3373 (1998)

[3] N. Katz, J. Egedal, W. Fox, A. Le, and M. Porkolab, *Physics Review Letters*, **101**, 015003 (2008)

[4] S.I. Krasheninnikov, *Physics Letters A*, **283**, 368-370 (2001)

[5] R.D. Hazeltine and J.D. Meiss, *Physics Reports*, **121**, Nos. 1 & 2 (1985).

[6] G. Fiksel, et al, *Plasma Sources Sci. Technol*, **5**, 78-83 (1996)

[7] I. Hutchinson, *Principles of Plasma Diagnostics*, Cambridge University Press, New York (2002).

[8] J.A. Bittencourt, *Fundamentals of Plasma Physics*, Springer-Verlag Inc., New York (2004).

[9] N. Katz, *Experimental Investigation of the Trigger Problem in Magnetic Reconnection*, Doctoral Dissertation, Massachusetts Institute of Technology, Dept. of Physics (2010).